Effect of anisotropic strain on the charge ordering transition in manganite films

Y. Z. Chen,[1] J. R. Sun,[1,a)] S. Liang,[1] W. M. Lv,[1] B. G. Shen,[1] and W. B. Wu[2]
[1]*State Key Laboratory of Magnetism and Beijing National Laboratory for Condensed Matter Physics, Institute of Physics, Chinese Academic of Sciences, Beijing 100080, People's Republic of China*
[2]*Hefei National Laboratory for Physical Sciences at the Microscale, University of Science and Technology of China, Hefei 230026, People's Republic of China*

(Received 18 January 2008; accepted 22 February 2008; published online 8 May 2008)

The substrate induced anisotropic strain was found to have a significant effect on the charge ordering (CO) transition and surface morphology in $Bi_{0.4}Ca_{0.6}MnO_3$ films deposited on (110)- and (111)-oriented $SrTiO_3$ substrates. Effects of film thickness t on the CO transition were further studied. The CO transition appears at T_{CO} when t exceeds 50 nm, and develops rapidly to an excellent state as t reaches 100 nm. The distinctive thickness-dependent CO transition has a close relation with the anisotropic strain relaxation process. © *2008 American Institute of Physics*. [DOI: 10.1063/1.2908222]

The charge- and orbital-ordered state in perovskite manganites has attracted a lot of interest for its colossal response to magnetic field, electric field, light, and pressure.[1] Because of the strong correlation between the charge- and orbital-ordered state and structure changes, a clear charge ordering (CO) transition has hardly been observed in manganite films[2] until the recent work by Nakamura *et al.*[3] and Wakabayashi *et al.*,[4] who used the (110)-oriented $SrTiO_3$ (STO) substrates for film growth. Films on the extensively used (100) substrates generally conserve a tetragonal distortion of the lattice. Though such distortion can drastically affect the film's electronic state,[5,6] it wipes out the clear CO transition during cooling.[2] While, for the films on the (110) substrates whose surfaces consist of rectangular meshes, the lattice mismatch could lead to a shear strain which accommodates the angular deviation from right angle. The shear strain makes it available for the concomitant changes of a and b axes required by the charge-ordered state, thus a possible clear CO transition as occurred in $Nd_{0.5}Sr_{0.5}MnO_3$.[3,4] In fact, besides the lattice strain induced by different substrates or different crystallographic orientations of the substrate, the strain relaxation process may also have an important impact on the physical properties of the manganite film. In (100) films, it has been found that the magnetic and transport properties significantly vary with the increase in film thickness,[7] and it is proposed that a 1% biaxial strain would cause a 10% shift in the Curie temperature T_C.[8] In addition to these, it has been well established that the concentration of mobile charge carriers can change in ultrathin films due to the presence of structural defects near the film-substrate interface,[9] which may also have a strong effect on CO transition.

By changing film thickness, both the lattice strain and carrier concentration can be tuned. Although it seems that the CO transition is independent of film thickness when the latter exceeds 80 nm, what will happen as film thickness is well 80 nm is still an open question, and a thorough investigation on this issue may give us the information on how to control the charge and orbital-ordered state in manganite films. Based on this consideration, in the present letter, we perform a systematic study on the effect of film thickness on CO transition. It is found that, for the films grown on the (110) STO substrates, the charge-ordered state emerges when film thickness exceeds 50 nm and rapidly develops when the film thickness increases from 50 to 100 nm. The distinctive thickness dependence of the CO transition is found to have a close relation to the strain relaxation along the [001] axis in the films. Interfacial effects may be unimportant considering the fact that they prevail only in the films below 10 nm.

$Bi_{0.4}Ca_{0.6}MnO_3$ (BCMO) films were prepared on (100), (110), and (111) STO substrates by the pulsed laser ablation technique following the procedures described elsewhere.[10] It should be mentioned that the films were found to show an average composition of $Bi:Ca:Mn \approx 0.41:0.59:1$, obtained by a careful energy-dispersive x-ray spectroscopy analyses. This is a composition very close to that of the target ($Bi:Ca:Mn \approx 0.43:0.57:1$). Structure analyses were performed by x-ray diffraction (XRD) on a Philips X'pert Pro diffractometer using Cu $K\alpha_1$ radiation. The surface morphology of the films was analyzed by atomic force microscopy (AFM) [Digital Instrument (DI) NanoScope IIIa]. Transport and magnetic measurements were performed on a physical property measurement system (PPMS-14h) and a superconducting quantum interference device magnetometer (MPMS-7), respectively.

Figures 1(a) and 1(b) show the temperature-dependent resistivity and magnetization of the films (~100 nm) on different oriented STO substrates. Data of the bulk counterpart are also presented for comparison. Both the (110) and (111) films show an obvious resistivity jump and a concomitant magnetization peak at T_{CO}, signifying the CO transition.[11,12] On the contrary, the film on (100) STO has no CO signature, as previously reported.[13] The CO transition in the (110) film is as sharp as that in the bulk material, but shows the lowest transition temperature $T_{CO} \sim 265$ K. In contrast, the (111) film exhibits a relatively broad CO transition and a higher

a)Author to whom correspondence should be addressed. Electronic mail: jrsun@g203.iphy.ac.cn.

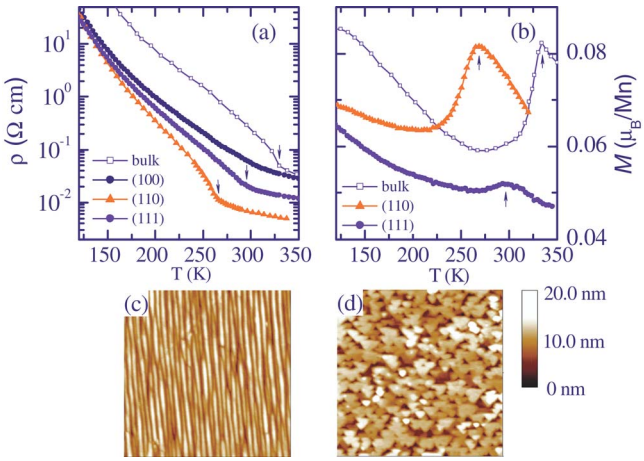

FIG. 1. (Color online) Temperature dependence of the resistivity (a) and magnetization (b) for the $Bi_{0.4}Ca_{0.6}MnO_3$ films on different oriented STO substrates and for bulk $Bi_{0.4}Ca_{0.6}MnO_3$. The arrows indicate the charge ordering transition. Shown in (c) and (d) are 2×2 μm^2 topographic images for (110) and (111) films, respectively.

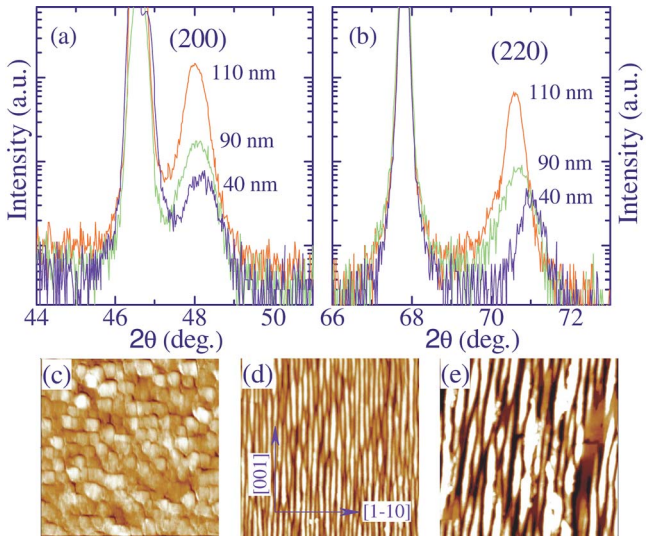

FIG. 2. (Color online) XRD linear scans around the (200) (a) and (220) (b) reflections for the (110) films. [(c)–(e)] the 2×2 μm^2 AFM images of the films with thicknesses of 40, 110, and 300 nm.

transition temperature $T_{CO}\sim300$ K. The results illustrate the profound effect of strain, induced by substrates with different crystallographic orientations, on the CO transition. In addition, the morphology of the films on different substrates is considerably different. The (100) film exhibits a surface consisting of tiny spherical grains (not shown), while the (110) and (111) films show a ridge-shaped and a triangular surface structure, respectively [shown in Figs. 1(c) and 1(d)]. These patterns reveal a crucial impact of substrate surface on film morphology. However, partial irregularity can be found in the surface of the (111) film, which should indicate its poor crystallinity as confirmed by the broad rocking curves (not shown) and may be the reason for its relatively broad CO transition. In contrast, the (110) films show a good crystallinity, and the regular ridgelike stripes should indicate its single domain structure as that in $La_{2-x}Sr_xCuO_4$ films.[14]

In the following, the (110) films with different thicknesses (10–300 nm) were systematically studied. Figures 2(a) and 2(b) show the XRD spectra of the (200) and (220) reflections for the BCMO films with the thicknesses of 40, 90, and 110 nm, respectively. It is obvious that, with the increase of film thickness, both the (200) and (220) peaks shift to lower angles, signifying the occurrence of strain relaxation. The obtained lattice constants as a function of film thickness are shown in Fig. 3.[15] For the 10 nm film, c is $\sim$0.3901 nm, whereas d_{1-10} is only $\sim$0.2698 nm ($\sim$0.2761 nm for STO), indicating a complete locking of the [001] axis, while a partial relaxation of the [1–10] axis resembling that in $Nd_{0.5}Sr_{0.5}MnO_3$ (Ref. 3). As the film thickness increases, the lattice strain relaxes, and $a=b=0.3795$ nm, $c=0.3836$ nm are obtained for a 300 nm film, similar to the previous report.[13] Furthermore, the film's surface morphology also evolves with increasing thickness. For the strongly strained 40 nm film, a mosaiclike surface structure is observed. As the strain relieved, regular ridges patterns ($\sim$50 nm in width) appear and the surface grows rather rough when film thickness exceeds 300 nm [Figs. 2(c)–2(e)].

Figure 4(a) shows the temperature-dependent resistance of the (110) films with different thicknesses. It can be seen that, for the 40 nm film, no signature of CO transition is observed, which may indicate a charge disordered (CD) state in the whole temperature range. As the thickness increases, CO transition appears and it swiftly develops to the most robust state in a $\sim$100 nm film. Further increasing the thickness, the sharp CO transition keeps while T_{CO} shifts to higher temperatures, showing the tendency to its bulk counterpart. In addition, for films thinner than 100 nm, an obvious increase of the resistivity at ambient temperature is observed as the thickness is decreased. For example, the resistivity of the 40 nm film is an order of magnitude higher than that of the 70 nm film. Since the thickness of the investigated film is much thicker than the film-substrate interface, the interface effect on the CO transition and the resistivity should be ruled out. Additionally, as shown in Fig. 2(c), the role of the discontinuous film coverage over the substrate surface should be also ruled out. Thus, the thickness-dependent CO transition and resistivity should be ascribed to strain variation, resulting from the strain relaxation process.

As investigated by the XRD measurements, the [001] and [1–10] axes sustain different strained states, thus asym-

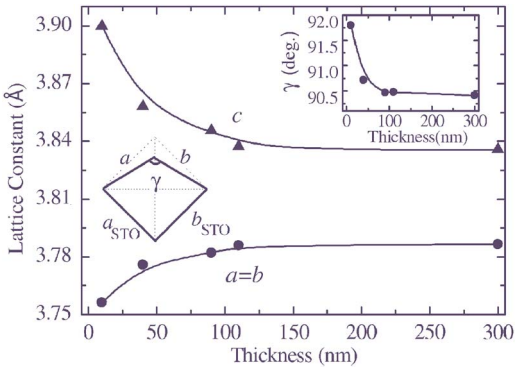

FIG. 3. (Color online) Thickness-dependent lattice constants of the (110) films. Shown in the interspace is the sketch of the strained film on the (110) STO. The inset shows the thickness-dependent γ, which denotes the lattice deviation from orthorhombic structure.

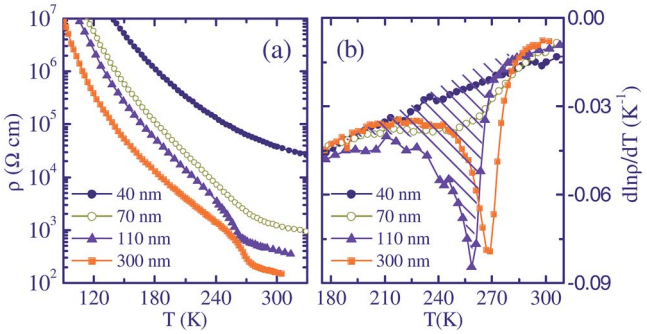

FIG. 4. (Color online) (a) Temperature-dependent resistance of the (110) films with different thicknesses. (b) thickness-dependent $d\ln\rho/dT$ around T_{CO}, the shaded area expresses the CO transition degree.

metric strain in the films. The anisotropic strain can be characterized by "orthorhombic" strains $Os_{\parallel}=2(b-a)/(b+a)$ in the a-b plane and $Os_{\perp}=|2(a+b-2c)/(a+b+2c)|$ along the c axis.[16] For $a\approx b$, $Os_{\parallel}$ keeps zero in all the films, indicating the lattice freedom in the $a-b$ plane. On the contrary, $Os_{\perp}$ exhibits obvious thickness dependence as shown in Fig. 5. Moreover, the normalized extent and degree of the CO transition as a function of film thickness are also shown in Fig. 5, which are determined by the area of the $d\ln\rho/dT$ peak around T_{CO} as demonstrated by the shaded area in Fig. 4(b). The thickness-dependent T_{CO}, the temperature where $d\ln\rho/dT$ takes the minimal value, is shown in the inset of Fig. 5. It is clear that, when c is tightly clamped by the substrate, an $Os_{\perp}$ maximum of ~0.038 is obtained and no CO transition is observed. As the relaxation along c axis happens, $Os_{\perp}$ correspondingly decreases. When $Os_{\perp}$ becomes half the maximum, CO transition appears. A robust CO state is obtained as $Os_{\perp}$ reaches ~0.014 (in the 100 nm film), about one-third of the maximum, which implies a strain relaxation of 2/3. Further increasing the film thickness leads to a slight variation of $Os_{\perp}$, and the resistive anomaly at T_{CO} remains essentially unaffected. The results indicate the presence of a close relation between the CO transition in the (110) films and the strain relaxation along the [001] axis. It should be mentioned that the highly strained c, that is, the elongation of the c axis, will inevitably lead to a decrease in the orbital overlap between Mn: e_g orbitals and O: $2p$ orbitals and hence provide a mechanism for the localization of the

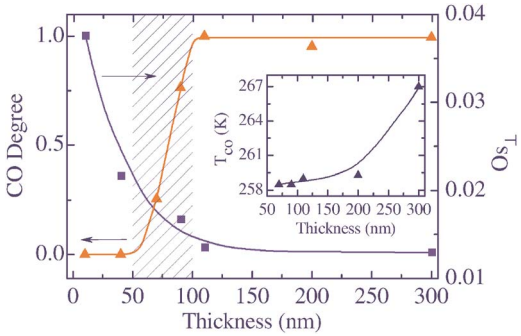

FIG. 5. (Color online) The normalized CO transition degree and the $Os_{\perp}$ strain as a function of film thickness. Inset: the thickness-dependent CO transition temperature T_{CO}.

conduction electron, which is compatible with the observed higher resistivity in thinner films at ambient temperature. On the other hand, a negligible increase of T_{CO} is observed with the thickness-dependent evolution of the CO transition, and the obvious increase of the T_{CO} in the 300 nm film may relate with the secondary surface morphology modification, as shown in Fig. 2(e). In addition, it can be seen that the evolution from the CD film to a robust CO one is achieved in a rather narrow range (~50 nm as illustrated by the shaded area in Fig. 5). In the critical region, partial relaxed states exist. Considering the strain effect on the configuration of charges and e_g orbitals, there may be some novel charge- and orbital-ordered structures as detected in $Nd_{0.5}Sr_{0.5}MnO_3$ (Ref. 4). Much more work will be needed in the future.

It is interesting that the observed phenomena are quite similar to the high-pressure-induced suppression of the CO transition and insulating behavior in the $Pr_{1-x}Ca_xMnO_3$,[17] which were thought to be resulted from the shear strains of the MnO_6 octahedra[18] or the monoclinic distortion evolving under high pressure.[16] The large deviation of γ from the right angle in the strained films (inset of Fig. 3), which displays the deviation from orthorhombic structure, implies the possible existence of monoclinic distortion induced by shear strain in our films.

This work has been supported by the National Natural Science Foundation of China and the National Basic Research of China.

[1] Y. Tokura and N. Nagaosa, Science **288**, 462 (2000).
[2] W. Prellier, A. Biswas, M. Rajeswari, T. Venkatesan, and R. L. Greene, Appl. Phys. Lett. **75**, 397 (1999).
[3] M. Nakamura, Y. Ogimoto, H. Tamaru, M. Izumi, and K. Miyano, Appl. Phys. Lett. **86**, 182504 (2005).
[4] Y. Wakabayashi, D. Bizen, H. Nakao, Y. Murakami, M. Nakamura, Y. Ogimoto, K. Miyano, and H. Sawa, Phys. Rev. Lett. **96**, 017202 (2006).
[5] Z. Fang, I. V. Solovyev, and K. Terakura, Phys. Rev. Lett. **84**, 3169 (2000).
[6] D. Gillaspie, J. X. Ma, H. Y. Zhai, T. Z. Ward, H. M. Christen, E. W. Plummer, and J. Shen, J. Appl. Phys. **99**, 08S901 (2006).
[7] G. Y. Gao, S. W. Jin, and W. B. Wu, Appl. Phys. Lett. **90**, 012509 (2007).
[8] A. J. Millis, T. Darling, and A. Migliori, J. Appl. Phys. **83**, 1588 (1998).
[9] M. Bibes, S. Valencia, Ll. Balcells, B. Martinez, J. Fontcuberta, M. Wojcik, S. Nadolski, and E. Jedryka, Phys. Rev. B **66**, 134416 (2002).
[10] Y. Z. Chen, J. R. Sun, D. J. Wang, S. Liang, J. Z. Wang, Y. N. Han, B. S. Han, and B. G. Shen, J. Phys.: Condens. Matter **19**, 442001 (2007).
[11] V. A. Bokov, N. A. Grigoryan, and M. F. Bryzhina, Phys. Status Solidi **20**, 745 (1967).
[12] W. Bao, J. D. Axe, C. H. Chen, and S.-W. Cheong, Phys. Rev. Lett. **78**, 543 (1997).
[13] D. H. Kim, H. M. Christen, M. Varela, H. N. Lee, and D. H. Lowndes, Appl. Phys. Lett. **88**, 202503 (2006).
[14] J. Kwo, R. M. Fleming, H. L. Kao, D. J. Werder, and C. H. Chen, Appl. Phys. Lett. **60**, 1905 (1992).
[15] As in the bulk material Ref. 11, a is similar to b. c is calculated through volume conservation. The angle between a and b, γ is deduced from $\cos(\gamma/2)=d_{110}/d_{100}$.
[16] D. P. Kozlenko, L. S. Dubrovinsky, I. N. Goncharenko, B. N. Savenko, V. I. Voronin, E. A. Kiselev, and N. V. Proskurnina, Phys. Rev. B **75**, 104408 (2007).
[17] C. W. Cui and T. A. Tyson, Phys. Rev. B **70**, 094409 (2004).
[18] A. Arulraj, R. E. Dinnebier, S. Carlson, M. Hanfland, and S. V. Smaalen, Phys. Rev. Lett. **94**, 165504 (2005).